Supporting information for the article

Complexes of Ni[II], Co[II], Zn[II], and Cu[II] with Promising Anti-Tuberculosis Drug: Solid-State Structures and DFT Calculations

Mohamed Ali Ahmed,[1,2] Maksim A. Zhernakov,[1] Edward M. Gilyazetdinov,[1] Mikhail S. Buharov,[1] Daut R. Islamov,[1,3] Konstantin S. Usachev,[3] Alexander E. Klimovitskii,[1] Nikita Yu. Serov,[1] Vladimir A. Burilov[1] and Valery G. Shtyrlin[1,*]

Kazan Federal University Kremlevskaya St., 18, Kazan, 420008, Russian Federation

E-mail: valery.shtyrlin@gmail.com

Table of content

Crystal structure

Table S1. Crystallographical data of the $^1_\infty\{[\text{Cu}\mathbf{L}\text{Cl}] \cdot 0.5\text{H}_2\text{O}\}$

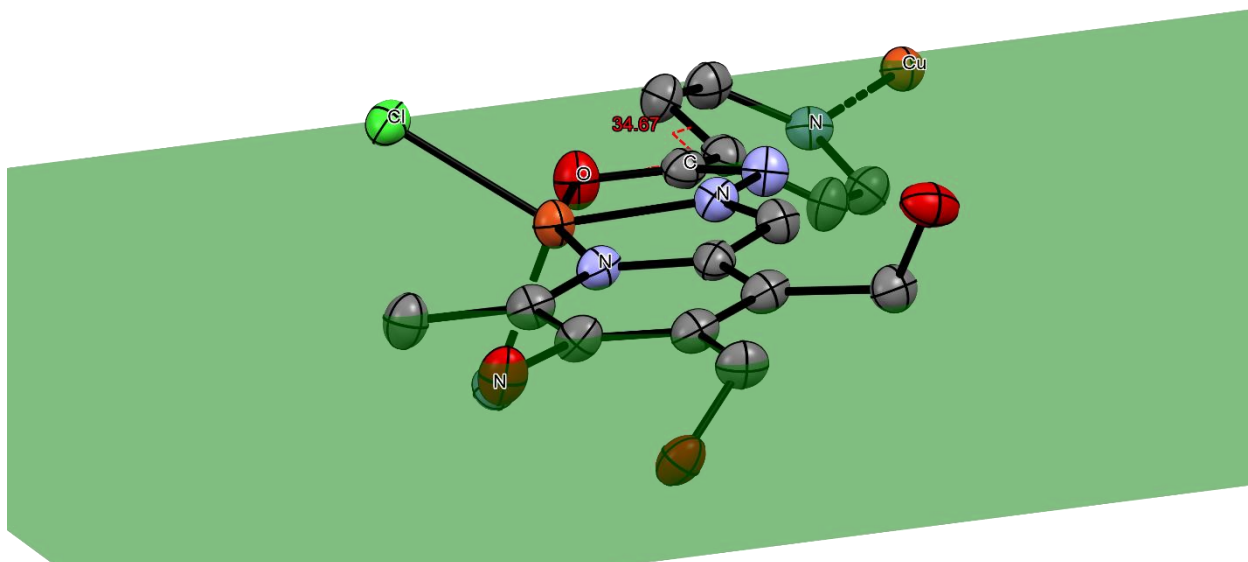| Compound	$^1_\infty\{[\text{Cu}\mathbf{L}\text{Cl}] \cdot 0.5\text{H}_2\text{O}\}$
Empirical formula	$C_{15}H_{16}ClCuN_4O_{4.5}$
Formula weight	423.31 g*mol^{-1}
Temperature	99.9(7) K
Wavelength	1.54184 Å
Crystal system	monoclinic
Space group	$P2_1/n$ (#14)
Unit cell dimensions	$a = 16.3539(11)$ Å, $b = 12.2647(6)$ Å, $c = 17.4916(10)$ Å, $\alpha = 90$ $\beta = 108.431(7)°$ $\gamma = 90°$
Volume	3328.4(4) Å^3
Z	8
Density (calculated)	1.689 g/cm^3
Absorption coefficient	3.636 mm^{-1}
$F(000)$	1728
Crystal size	0.05 x 0.20 x 0.31 mm^3
Theta range for data collection	$8.95° \leq 2\Theta \leq 153.062°$
Reflections collected	17815
Independent reflections	6353
Goodness-of-fit on F^2	1.132
Final R indices [I>2σ(I)]	0.0680
R indices (all data)	0.1640
Largest diff. peak and hole	1.014 and –0.686 e.Å^{-3}

Figure S1. Planar view of $\frac{1}{\infty}\{[Cu\mathbf{L}Cl] \cdot 0.5H_2O\}$.

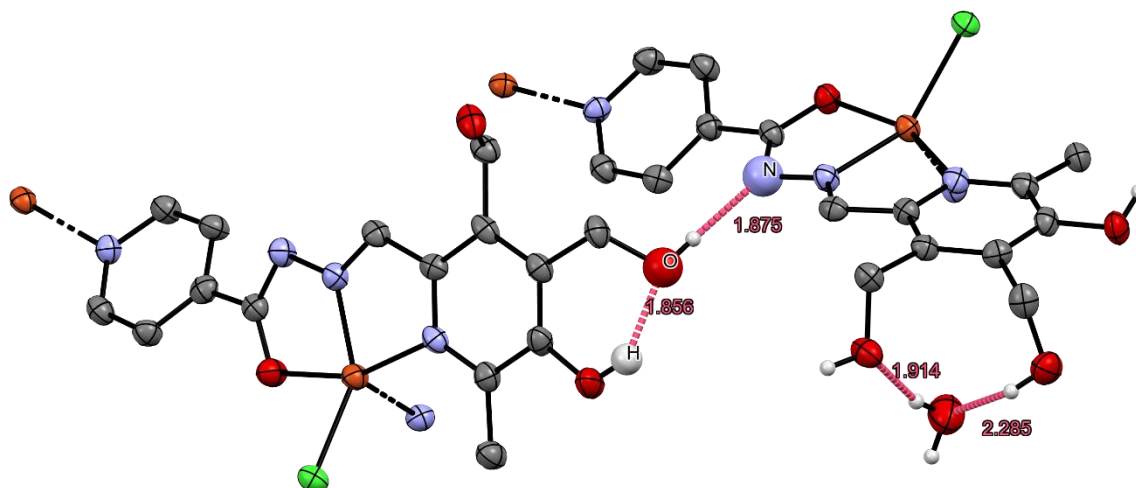**Figure S2**. System of the H-bonds for $\frac{1}{\infty}\{[Cu\mathbf{L}Cl] \cdot 0.5H_2O\}$.
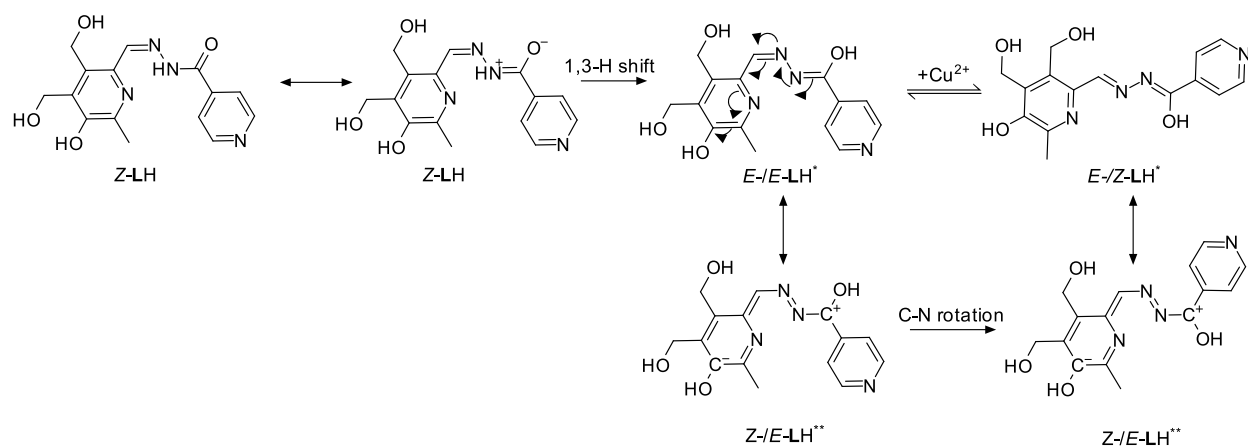
Isomeric conversion

Figure S3. Possible isomeric conversion of the **LH** ligand in solution.
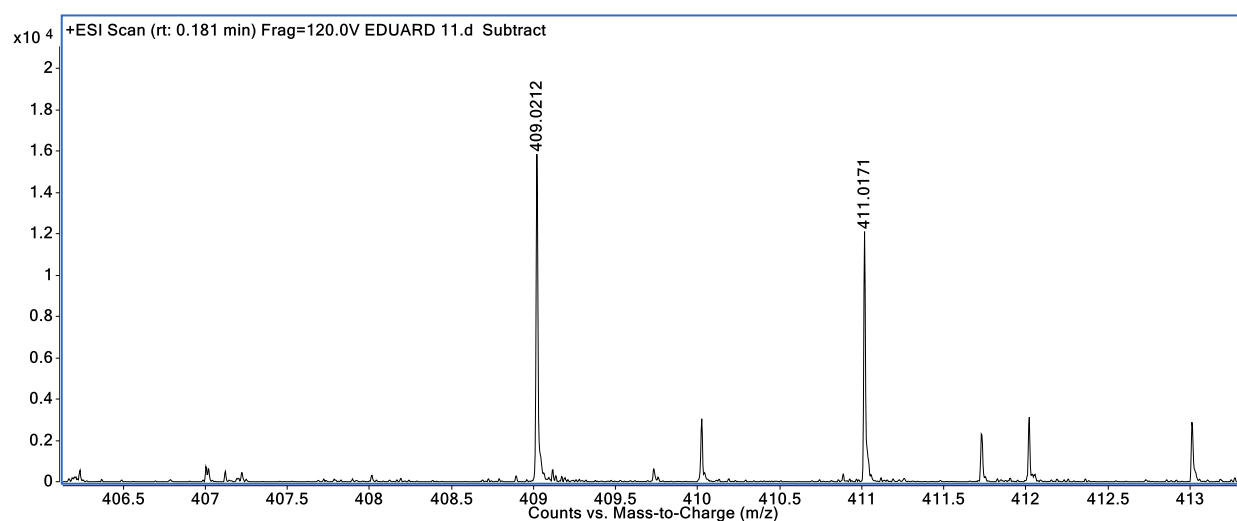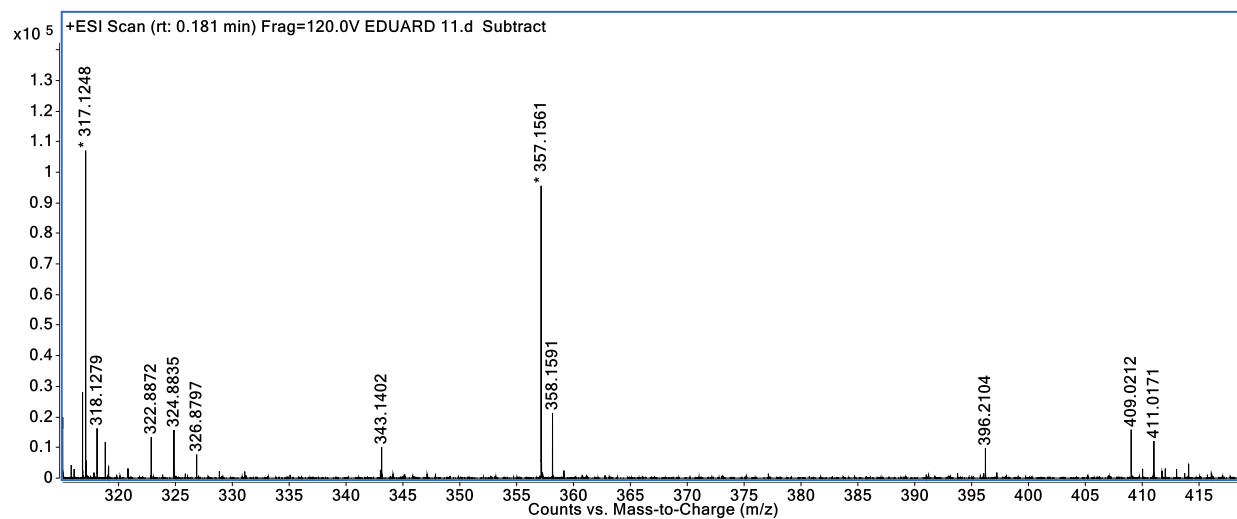
Mass-spectrometry
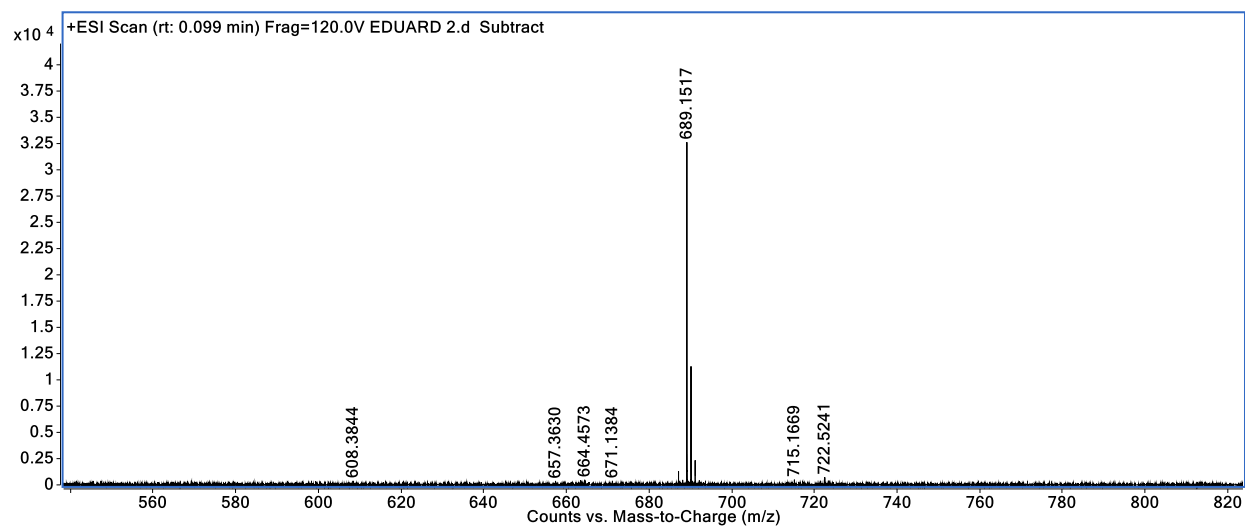

Figure S4. Mass spectra of the Ni-**LH** complex.

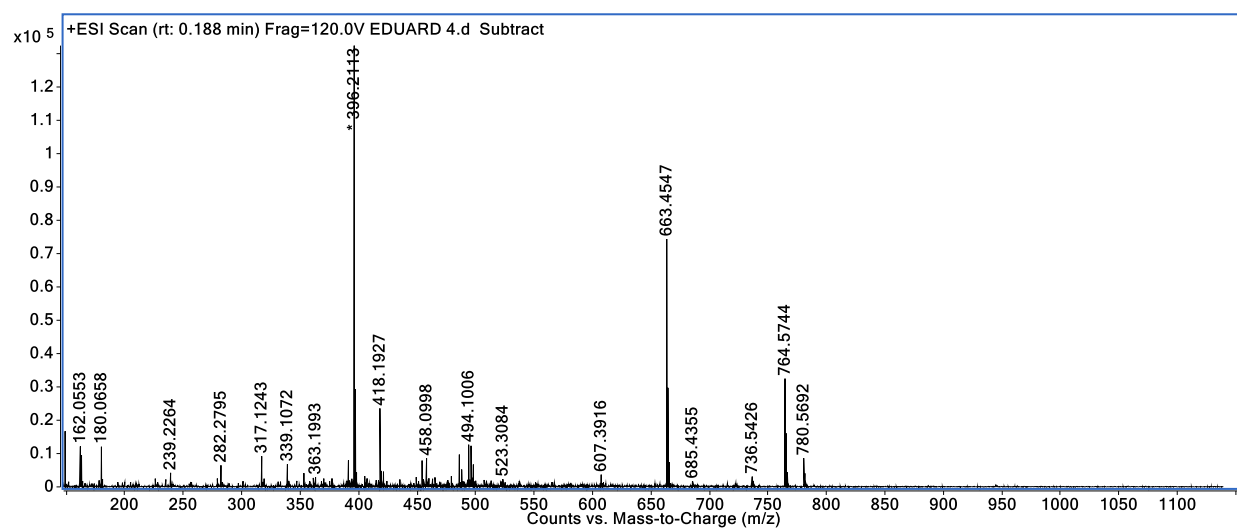**Figure S5**. Mass spectrum of the Co-**LH** complex.

Figure S6. Mass spectrum of the Zn-**LH** complex.
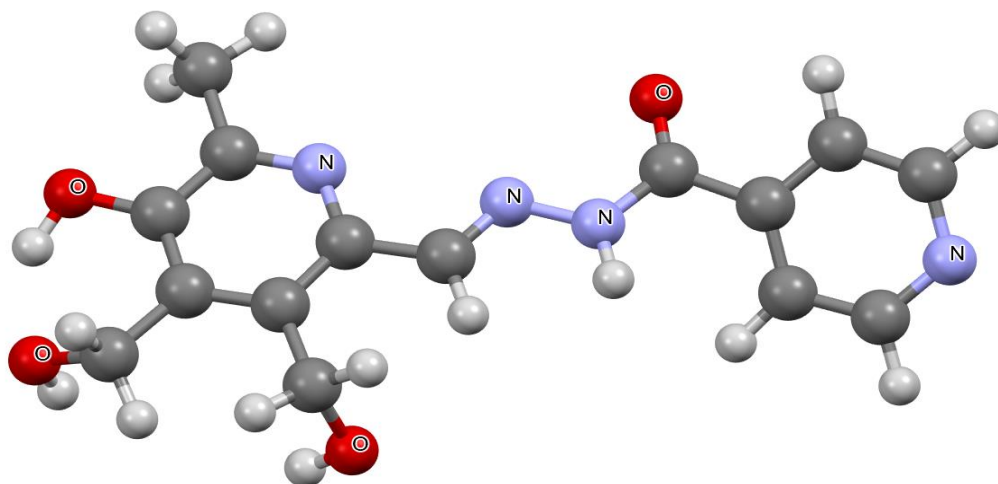
DFT calculations

Figure S7. Structure and formation energy (in atomic units, a.u.) of *E*-**L**H conformer optimized on the B3LYP/def2-TZVPP level with accounting solvent effects in the C-PCM model and dispersion correction (D3BJ), *E* = −**1101.03435 a.u.**
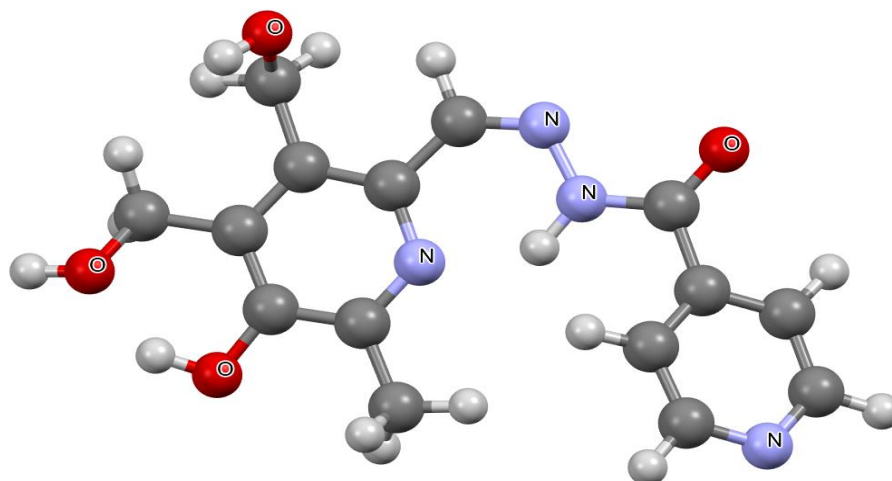

Figure S8. Structure and formation energy (in atomic units, a.u.) of *Z*-**L**H conformer optimized on the B3LYP/def2-TZVPP level with accounting solvent effects in the C-PCM model and dispersion correction (D3BJ), *E* = −**1101.03921 a.u**.

Figure S9. Structure and formation energy (in atomic units, a.u.) of *Z*-**L**H conformer optimized on the B3LYP/def2-TZVPP level with accounting solvent effects in the C-PCM model and dispersion correction (D3BJ), $E = -1101.03518$ **a.u.**
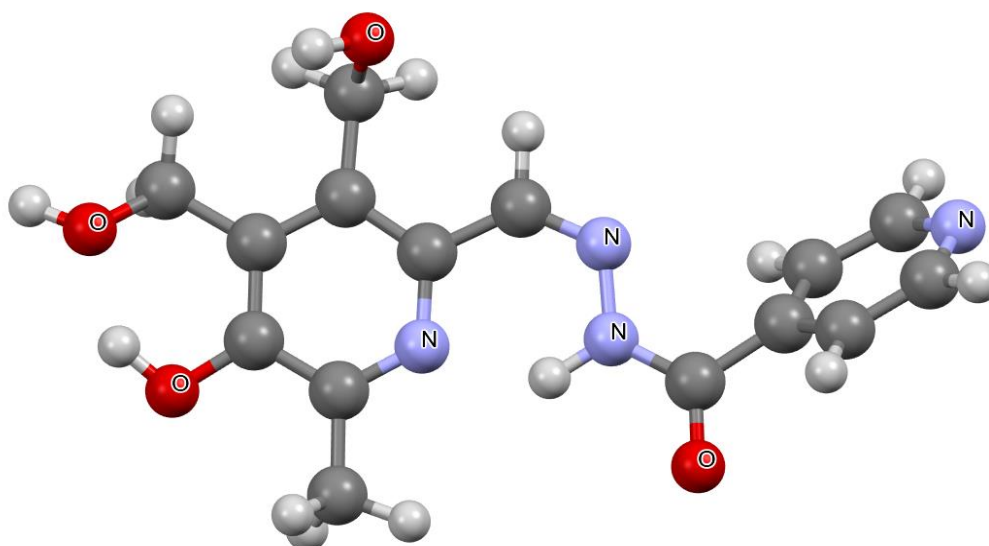

Figure S10. Structure and formation energy (in atomic units, a.u.) of *Z*-**L**H conformer optimized on the B3LYP/def2-TZVPP level with accounting solvent effects in the C-PCM model and dispersion correction (D3BJ), $E = -1101.03257$ **a.u**.
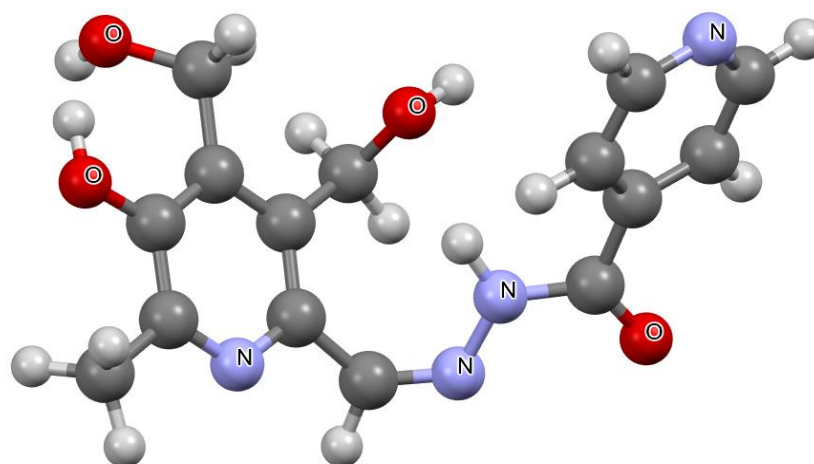
Figure S11. Structure and formation energy (in atomic units, a.u.) of *Z*-**L**H optimized on the B3LYP/def2-TZVPP level with accounting solvent effects in the C-PCM model and dispersion correction (D3BJ), $E = -1101.02839$ **a.u.**
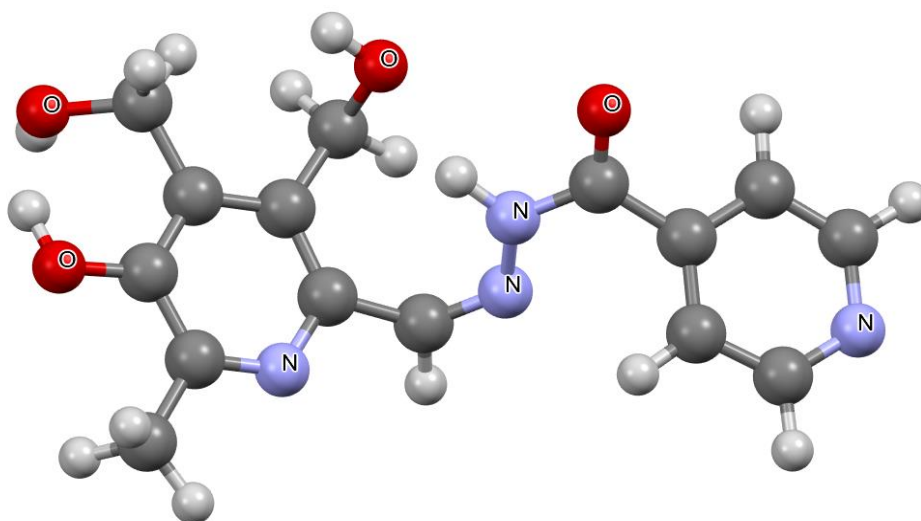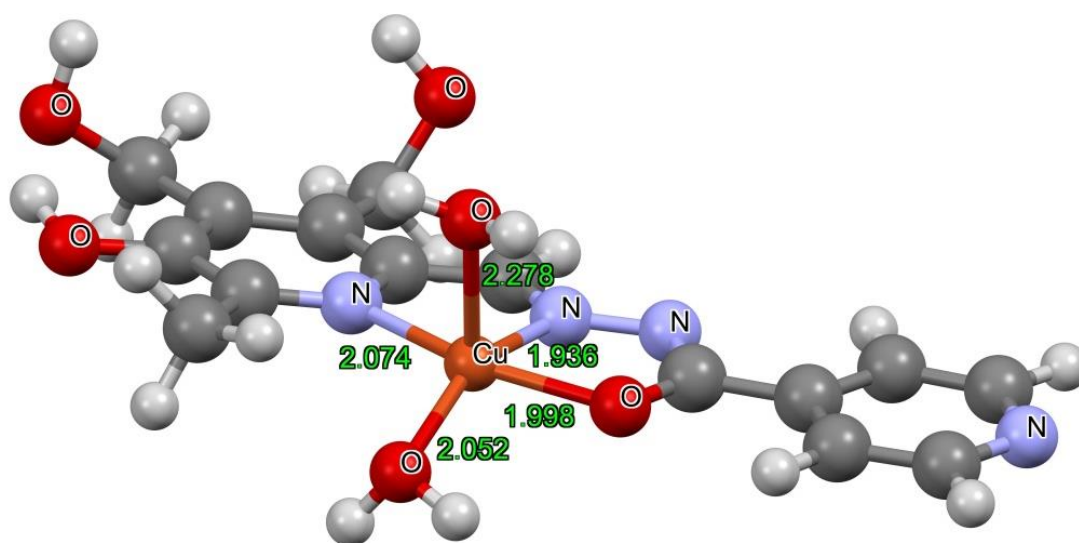

Figure S12. Structure of [Cu**L**(H$_2$O)$_2$] complex and selected interatomic distances optimized on the B3LYP/def2-TZVPP level with accounting solvent effects in the C-PCM model and dispersion correction (D3BJ).

Figure S13. Structure of [Cu**L**(H$_2$O)Cl] complex and selected interatomic distances optimized on the B3LYP/def2-TZVPP level with accounting solvent effe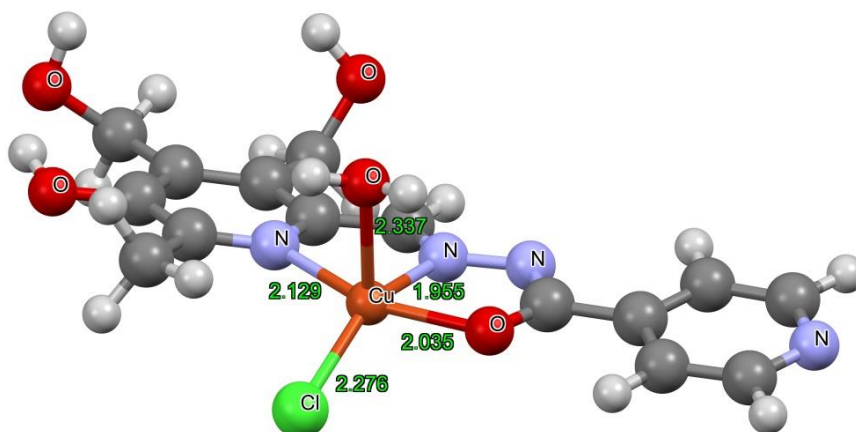cts in the C-PCM model and dispersion correction (D3BJ).